Journal of ELECTRONIC MATERIALS
https://doi.org/10.1007/s11664-018-6289-3

Preparation and Characterization of Biomass-Derived Advanced Carbon Materials for Lithium-Ion Battery Applications

ANDRI HARDIANSYAH,[1,7] ELSY RAHIMI CHALDUN,[2] BEBEH WAHID NURYADIN,[3] ANTI KHOERUL FIKRIYYAH,[3] ACHMAD SUBHAN,[4] MUHAMMAD GHOZALI,[5] and BAMBANG SUNENDAR PURWASASMITA[6]

1.—Department of Metallurgy and Materials Engineering, Faculty of Engineering and Design, Bandung Institute of Technology and Science, Bekasi 17530, Indonesia. 2.—Research Unit for Clean Technology, Indonesian Institute of Sciences, Bandung 40135, Indonesia. 3.—Department of Physics, Universitas Islam Negeri Sunan Gunung Djati, Bandung 40614, Indonesia. 4.—Research Center for Physics, Indonesian Institute of Sciences, Tangerang 15314, Indonesia. 5.—Research Center for Chemistry, Indonesian Institute of Sciences, Tangerang 15314, Indonesia. 6.—Advanced Material Processing Laboratory, Department of Engineering Physics, Bandung Institute of Technology, Bandung 40132, Indonesia. 7.—e-mail: asprakkidas@yahoo.com

In this study, carbon-based advanced materials for lithium-ion battery applications were prepared by using soybean waste-based biomass material, through a straightforward process of heat treatment followed by chemical modification processes. Various types of carbon-based advanced materials were developed. Physicochemical characteristics and electrochemical performance of the resultant materials were characterized systematically. Scanning electron microscopy observation revealed that the activated carbon and graphene exhibits wrinkles structures and porous morphology. Electrochemical impedance spectroscopy (EIS) revealed that both activated carbon and graphene-based material exhibited a good conductivity. For instance, the graphene-based material exhibited equivalent series resistance value of 25.9 Ω as measured by EIS. The graphene-based material also exhibited good reversibility and cyclic performance. Eventually, it would be anticipated that the utilization of soybean waste-based biomass material, which is conforming to the principles of green materials, could revolutionize the development of advanced material for high-performance energy storage applications, especially for lithium-ion batteries application.

Key words: Soybean waste, activated carbon, graphene, electrochemical properties

INTRODUCTION

Carbon-based advanced materials are widely developed due to their unique and excellent properties. A wide variety of carbon structure and morphology could be synthesized through various techniques including the chemical vapor deposition process,[1] catalytic pyrolysis,[2] carbonization, and chemical activation.[3–5] Recently, carbon-based advanced materials have been developed for numerous applications including electrochemicals,[5] electronics,[6] drug delivery systems,[7] electro-catalytic supports,[8] lithium-ion batteries,[9] and supercapacitors.[3,10,11] In respect to the electronic and energy storage applications, various types of carbon materials including activated carbons,[5,9] aerogels,[12] carbon nanotubes,[12] graphene,[13,14] and graphene composites[15,16] have been developed as important components in electronic devices due to their appropriate structures and surface area, which are accessible to the electrolyte, and their high electrical

(Received July 17, 2017; accepted April 6, 2018)

Published online: 25 April 2018

conductivity. The graphene-based materials have attracted scientists and researchers across the world due to their unique and specific properties that could revolutionize the development of advanced electronic materials. Graphene can be obtained through the exfoliation of graphite via a chemical modification process. Interestingly, in the last few years, graphene-based materials have been developed as a promising component in lithium-ion batteries.[17–24]

Commonly, the main sources for the preparation of carbon-based advanced materials have a high cost of raw materials which limit the further applications. Thus, the research for an effective and efficient strategy is needed to achieve the acceleration in the development of low cost and high-performance energy storage materials. Biomass is an abundant and renewable potential material source for producing advanced materials. A high amount of biomass with less or no economic value can be used as an inexpensive and efficient carbon precursor source for the preparation of advanced functional materials with high added-value both technologically and economically. The structure, morphology, and surface chemical composition of the carbon precursor material highly affect its applications. The previous study has explored some natural resources including rice husk,[9] kelp,[4] human hair,[25] loofa sponge,[3] bamboo,[5] chicken feathers,[26] honey,[27] coconut shells,[10] sewage sludge,[28] and cotton[12] as the main precursor material for electronic and energy storage applications. Specifically, soybean waste, a widely available and inexpensive biomass shows a promising application for development of carbon-based advanced materials. This material can be considered as a natural product-based waste, which is produced immediately after the extraction from the soybean or by as-product of food processing such as tofu, the main food in South East Asia countries, such as Indonesia.[29]

In the present work, we report the preparation and evaluation of carbon-based advanced material by using soybean waste as a precursor via the simple and easy process of heat treatment of carbon precursor followed by several chemical-triggered processes. The resultant structures and morphology were evaluated by scanning electron microscopy (SEM), transmission electron microscopy (TEM), x-ray diffraction (XRD), and Fourier-transform infrared (FTIR) spectroscopy. Electrochemical performance and its electronic characteristics for the resultant carbon-based advanced materials were investigated through cyclic voltammetry (CV), galvanostatic charge/discharge (CD), and electrochemical impedance spectroscopy (EIS) measurements.[30] Its potential applications for electronic and energy storage components, especially for the lithium-ion battery were elaborated.

EXPERIMENTAL PROCEDURES

Materials

Fresh soybean curd waste was collected from an as-product of a tofu processing factory (Bandung City, Indonesia), and the remaining water from the soybean waste was removed by drying at 70°C. Potassium hydroxide (KOH), hydrogen peroxide (H_2O_2), potassium permanganate ($KMnO_4$), sulfuric acid (H_2SO_4), hydrochloric acid (HCl), nitric acid (HNO_3), polyvinylidene fluoride (PVDF), acetylene black, and dimethylacetamide (DMAC) were purchased from Merck, Germany. Lithium hexafluorophosphate ($LiPF_6$) and ethylene carbonate/diethyl carbonate (EC/DEC) were purchased from Sigma-Aldrich. High-purity water purified by a Milli Q Plus water purifier system (Millipore, USA), with a resistivity of 18.3 MΩcm was used in all experiments. All the chemicals were used without further purification.

Carbonization and Activation Process

The carbonaceous materials were developed from soybean waste through a carbonization process as a method previously developed with minor modification.[31] This method involved several main processes including the cleaning process, carbonization and followed by the purification of as-prepared sample. Briefly, the soybean curd residue was washed carefully with deionized water to remove any impurities and dried at 100°C for 24 h. About 10 g of soybean curd residue was transferred into a porcelain boat and carbonized under high purity nitrogen flow atmosphere at 700°C in a horizontal tube furnace for 2 h. The sample was then washed several times with distilled water it until reached pH 7 and dried at 70°C for 24 h. The resulting product was denoted as non-activated carbon and then preserved in a sealed-glass tube at room temperature prior to characterizations. Furthermore, non-activated carbon was chemically activated using KOH as the method described previously with minor modification.[3] Briefly, the non-activated carbon was mixed uniformly with KOH (alkali/carbon ratio of 4). The resulting sludge was dried and then subjected to a porcelain boat for the activation at 700°C for 2 h. The resultant black powder was then immersed in HCl solution to remove any impurities and subsequently washed with deionized water. The sample was dried *in vacuo* for 24 h. The resulting product was denoted as activated carbon and then preserved in the sealed-glass tube at room temperature prior to characterizations.

Graphitization Process and Preparation of Graphene-Based Materials

Preparation of graphene-based materials from biomass-based materials involved two main steps as described previously with minor modification.[32] The process involved the graphitization process of carbonized material and the transformation process of graphitic material into graphene-based materials by using Hummer's method with minor modification. Briefly, 1 g of carbonized materials and

$FeCl_3 \cdot 6H_2O$ were mixed uniformly using distilled water. The pH of the sludge was adjusted to pH 2 by adding HCl. The mixture was stirred at 60°C for 5 h, then left for one week at room temperature. Further, the sample was dried at 100°C for 5 h to obtain a black solid material. The resulting product was denoted as graphitic carbon. The obtained graphitized materials were ground by a mortar to obtain powders that were used in the next step. Afterwards, graphene oxide was prepared using as-prepared flake expandable graphite as the precursor material via a modified Hummer's method with minor modification.[33] Briefly, a graphite flakes powder was added into concentrated H_2SO_4 and stirred uniformly for 1 h. Further, the beaker was put into an ice bath followed by adding concentrated HNO_3 to the mixture. Furthermore, $KMnO_4$ was slowly added into the mixture, which was vigorously stirred and with continued stirring for 5 days. Afterwards, an amount of water was added slowly and with continued stirring for 2 h. In the next step, H_2O_2 was slowly added and with continued stirring for 2 h and left for 24 h to precipitate the graphene oxide. Further, the supernatant was removed followed by adding distilled-water, H_2O_2, and HCl then continued with stirring for 2 h to terminate the reaction. Finally, the resulting suspension of graphene oxide was centrifuged at 4500 rpm. This process was conducted three times. The final suspension was washed until pH neutral was achieved. The product was dried at 40°C *in vacuo* which resulted in graphene oxide powder. The unique part of the aforementioned methods is a simultaneous procedure in order to develop a variety carbon-based material derived from biomass materials through heat treatment and a chemical-based process. These procedures might be developed for another variety of biomass materials.

Materials Characterizations

Structure and morphology of carbon-based advanced materials were characterized by scanning electron microscopy (SEM JEOL JSM-6390) and TEM (TEM FEI Tecnai G2 20 S-Twin). XRD was conducted using a D_2 Phaser BRUKER x-ray powder diffractometer to evaluate the crystallinity of the resultant materials by scanning dried powder with Cu $K_{\alpha-1}$ (1.5406 Å) radiation. The infrared spectrum was analyzed using a FTIR (Agilent Cary 630 FTIR Spectrometer) to determine the major functional groups of the resultant materials.

Fabrication and Assembly of Electrode Cell

The electronic and electrochemical characteristics of the resultant materials were further investigated using an electrode cell testing device. Prior to the cell assembly, the main component materials including cathode, anode, and electrolyte were prepared. The electrodes material was fabricated by mixing the as-prepared carbon materials (non-activated carbon, activated carbon, graphitic carbon or graphene) as the active material (85 wt.%), polyvinylidene fluoride (PVDF) as polymer binder (10 wt.%) and acetylene black, as a commercial carbon black (5 wt.%) in dimethylacetamide (DMAC) solution until it formed a homogeneous slurry. The slurry was coated on Cu foil (thickness 20 μm) with the layer thickness controlled to be $\pm$ 200 μm followed by drying at 80°C for 12 h in an oven. Furthermore, the electrochemical test was conducted using a CR2032 stainless steel coin cell. The electrolyte composition was 1 M $LiPF_6$ in a 1:1 mixture of EC/DEC. Briefly, the as-prepared electrode was combined with other components to develop a sandwich structure. Lithium metal was used as the counter electrode and polypropylene (Celgard 2500, Celgard Inc., USA) was used as the separator. Prior to the application, Celgard was wetted by using electrolyte. The assembly of the test cells was carried out in an argon-filled glove box in order to protect the assembly process against impurities.

Electrochemical Characterization

The electrochemical properties of the resultant materials were characterized by CV, CD, and EIS measurements. The CV test was conducted using a voltage between 0.1 V and 2.3 V at a single scan rate of 100 μVs^{-1}. The CV of coin cells was conducted at a half state of charge using Li/as-prepared carbon material electrodes as the working electrode and lithium electrode as both reference and counter electrode. CD tests of coin cells were measured with a constant current at a voltage ranging from between 0.1 V and 2.3 V (versus Li/Li^+) on a WBCS3000 cell test apparatus at room temperature. Moreover, the EIS test was performed by applying 20 mV AC voltage amplitude with the frequency ranging from 20 kHz to 0.1 Hz. EIS of coin cells was conducted at a half state of charge using Li/as-prepared carbon material electrodes as the working electrode and la ithium electrode as both reference and counter electrode.

RESULTS AND DISCUSSION

Characterizations of Structure and Morphology

Figure 1 shows SEM images of pristine soybean waste (a), non-activated carbon (b), activated carbon (c) graphite (d), and graphene (e). Structurally, pristine soybean waste (Fig. 1a) and non-activated carbon (Fig. 1b) exhibit many obvious wrinkles, significant pores with different pore sizes, and also interconnected structures. As seen in Fig. 1c, the activated carbon products possess a similar morphology with the non-activated carbon. Additionally, the KOH-activated process contributed to the enhancement of the pore volume, enlarginge the diameter of the pores and increasing the porosity.[34]

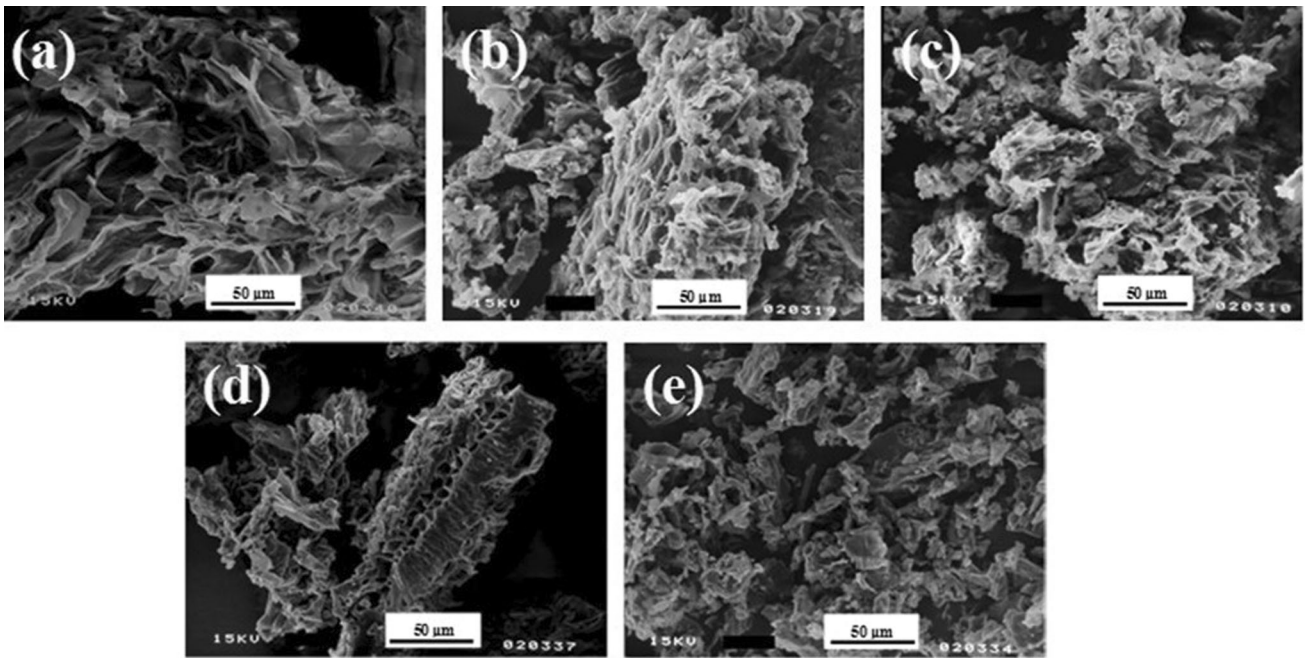

Fig. 1. SEM images of (a) pristine soybean waste, (b) non-activated carbon, (c) activated carbon, (d) graphitic carbon, and (e) graphene.

All of these phenomena are probably caused by the release of residual gases during the carbonization process at high temperature. At the high temperature, KOH could react with carbon to generate hydrogen, carbon dioxide and carbon monoxide gas, and thus the pores are created. Development of microporous and mesoporous-based structures could provide an easy ways for the movement of the electrolyte ions which indicate that this carbonized material could be promising for advance electrode materials. Furthermore, Fig. 1d and e show the graphite carbon and graphene material derived from the further processing of carbonized material and graphitized material, respectively. The surface morphology of the graphene appears as a layered structures (Fig. 1e). This is in accordance with previously reported investigations.[22]

TEM images are shown in Fig. 2a–c. Figure 2a shows a TEM image of non-activated carbon material. According to the TEM image, it can be seen that non-activated carbon materials are composed of an agglomeration of disordered amorphous carbon. Figure 2b shows a TEM image of activated carbon material. From the TEM image, it can be seen that the activated carbon material is composed of many porous structures due to the activation process by KOH. Furthermore, the TEM image of graphene material (Fig. 2c) revealed the formation of a few layered graphene material structures due to the chemical exfoliation process of graphite materials. The TEM results are in agreement with the SEM results. This result is in accordance with the previously developed biomass-derived graphene materials.[35,36]

Crystallographic analysis of the various carbon-based advanced materials was investigated by XRD analysis. XRD spectrum of the non-activated carbon, activated carbon, and graphene material are shown in Fig. 2d-1, d-2, and d-3, respectively. The XRD spectrum in Fig. 2d-1 shows a broad peak around 2θ of 25.1° (002) and 2θ of 43.2° (100) which is typically spectrum of amorphous carbonaceous material.[9] The peaks at 2θ around 29°, 31° and 33° indicated the spectrum from polysaccharide-based substances that might be derived from the soybean. The XRD spectrum in Fig. 2d-2 shows a broad peak around 2θ of 26° and a weak peak at around 2θ of 43.3° indicated the disordered nature and stacking of agglomerated carbon sheets, respectively.[9] XRD spectra of activated carbon have not introduced any oxides. This confirms that KOH-derived impurities have been removed completely through the purification processes. The diffraction peaks relatively weaken after chemical activation compared with the non-activated carbon, which indicates the destruction of the graphite layer alignment by KOH. Based on this result, through the chemical activation process, we could develop the amorphous activated carbon materials. Moreover, Fig. 2d-3 shows the XRD pattern of graphene. The appearance of a broad peak at around 2θ of 25° is assigned to the (002) characteristic diffraction of the two co-existences of amorphous graphitic carbon. Additionally, the appearance of a broad peak is observed at around 2θ of 25° and 43.1° of diffraction of the (002) and (100) planes of the hexagonal graphitic carbon, respectively. This indicates that the resultant of carbonized material is the turbostratic disordered

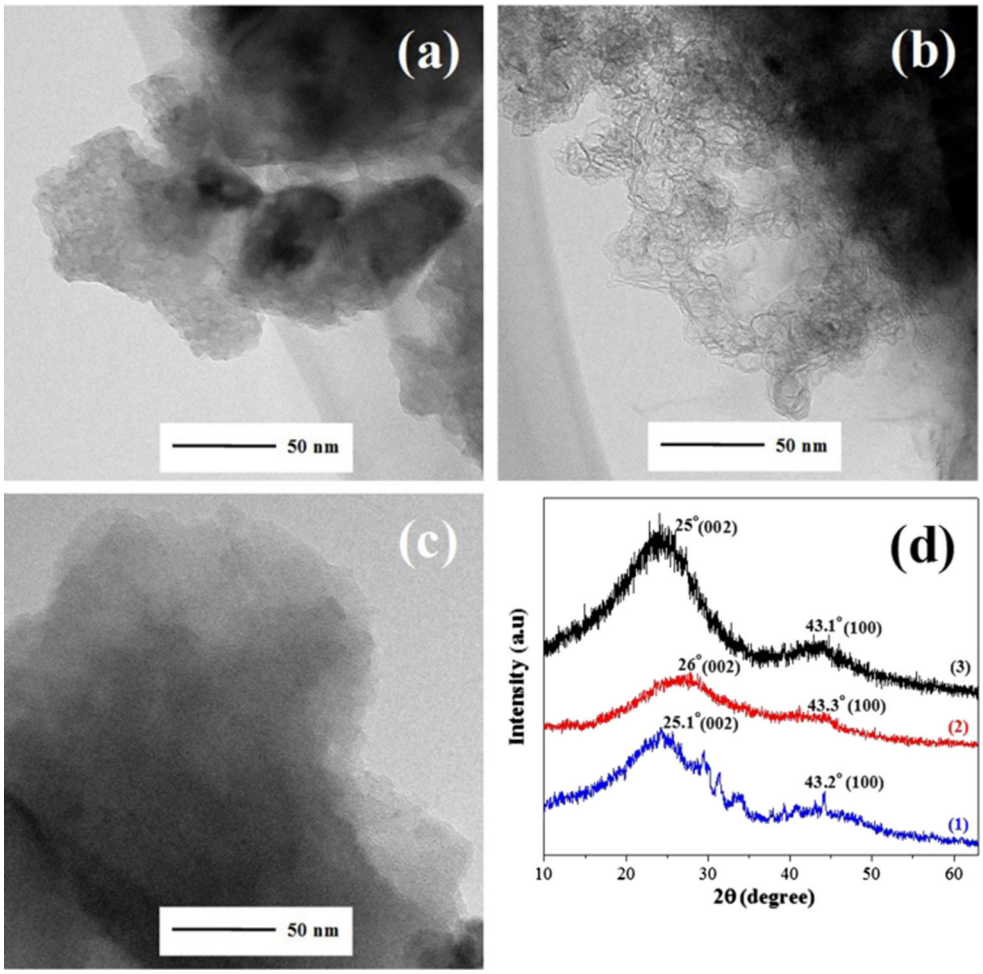

Fig. 2. TEM images of (a) non-activated carbon, (b) activated carbon, (c) graphene, and (d) XRD spectrum of (1) non-activated carbon, (2) activated carbon, and (3) graphene.

carbon with a low degree of crystallinity between graphite and amorphous carbon. The broad nature of the peak indicates a disordered structure created during synthesis by the modified Hummer's method. This result is in accordance with the previous investigations.[17]

Based on the FTIR spectrum, the pristine soybean waste has been transformed into different structures after the carbonization process. Figure 3a shows various functional groups for pristine soybean waste which are contained in more functional groups than the carbonized material. The pristine soybean waste presents hydroxyl functional groups, including hydroxyl (O–H) stretching around 3500 cm^{-1} to 3300 cm^{-1}, which is much less prevalent in the carbonized materials (Fig. 3b, c and d). The reduction of hydrogen bonding indicates that the KOH acts as a dehydrating agent, which reacted with the pristine soybean waste. The intense band at 2920 cm^{-1} is assigned to asymmetric C–H stretching which is reduced in carbonized materials. This further confirms that the activation removed a significant amount of hydrogen. Furthermore, the intense peak at 1740 cm^{-1} present in the pristine soybean waste indicated the carbonyl (C=O) stretching absorption. This peak was also absent in the carbonized materials which are indicated such that the carbonization and chemical activation could destruct aliphatic and aromatics bonds and removed volatile substances. Graphene material exhibit peaks at 1180 cm^{-1} and 1545 cm^{-1} indicating the C-O vibration and vibration of the skeleton of graphene, respectively. Furthermore, these results confirm the transformation of soybean waste-based material into the advanced functional materials for developing long-term sustainable energy storage devices and contribute to the development of a green environment through the reduction of waste.

Electrochemical Performance Characteristics

The electrochemical characteristics and cycling performance of these carbon-based advanced materials as an electrodes device was characterized through CV, CD, and EIS spectroscopy by using 1 M of $LiPF_6$ EC/DEC electrolyte. Figure 4 shows

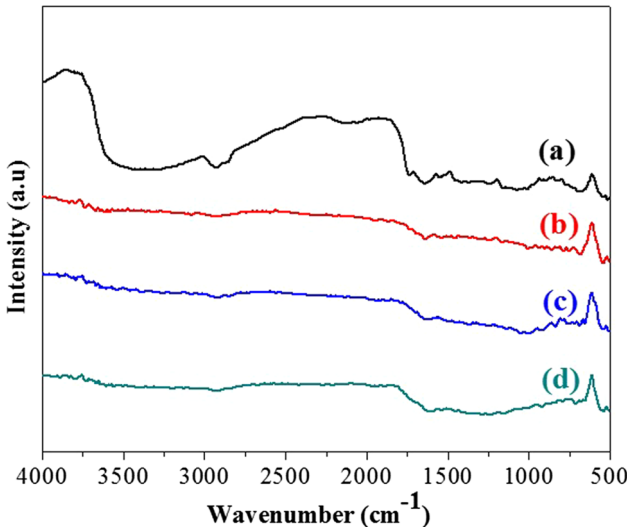

Fig. 3. FTIR spectrum of (a) pristine soybean waste, (b) non-activated carbon, (c) activated carbon, and (d) graphene.

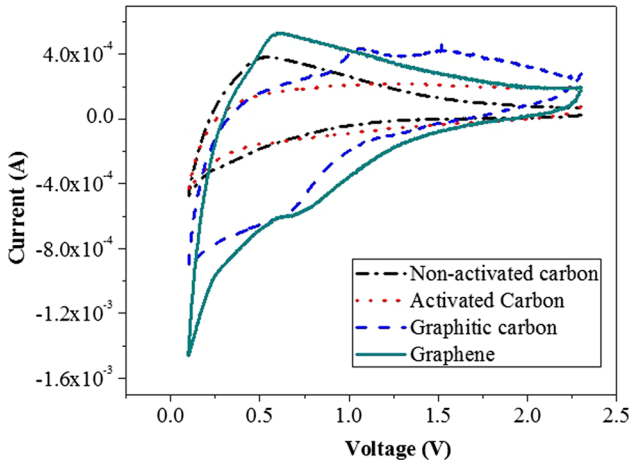

Fig. 4. Cyclic voltammogram of non-activated carbon, activated carbon, graphitic carbon, and graphene.

the CV profile of the various carbon structures. Generally, the cyclic voltammogram shows a quasi-rectangular shape with slight distortion. As shown in Fig. 4, cathodic and anodic peaks were observed of the various carbon structures. CV curve of graphene-based materials exhibited higher specific cathodic current compared with non-activated carbon, activated carbon, and graphitic carbon. Cathodic peaks could be detected during the first lithiation and intercalation process. Generally, the broad oxidation peaks in the CV curve were observed for carbon-based structures. These phenomena might be related to the less crystallinity of the developed carbon materials, as confirmed by XRD analysis. The CV curve of graphene-based materials exhibited the peak around 0.7 V that could be attributed to the intercalation process of lithium into the layers of graphene. Furthermore, the stronger peak during the lithiation process indicated more active intercalation sites existed in graphene material. This might be due to the synergetic interaction between lithium and the residual oxygen-containing functional groups on the graphene surface. These cathodic peaks indicated the electrolyte decomposition which followed by the formation of solid electrolyte interface (SEI) layer formed on the surface of the electrode.[23] In the anodic scanning process of graphene material, a peak around 0.4 V until 0.6 V can be observed. This peak was attributed to the delithiation mechanism of lithium in graphene material. This is in accordance with the previously reported research.[14,17,37]

Figure 5 shows the first galvanostatic charge/discharge profiles at a current density of 0.2C (the theoretical capacity was 1C corresponding to 372 mAg^{-1} as for a graphite electrode). Generally, the galvanostatic charge/discharge characteristics of graphene materials were higher than graphitic carbon, activated carbon and non-activated carbon. These phenomena might be due to the acceleration of the diffusion process of lithium ions into the host position of graphene sheets with fewer layers and porous structures. Additionally, more activation lithium-ion sites that developed on the surface of graphene materials would enhance the electrochemical performance of the graphene-based material. These results are in accordance with the previously reported results.[14,16] The first charge and discharge value of non-activated carbon (C–C′) and activated carbon (AC–AC′) were 90 $mAhg^{-1}$ and 97 $mAhg^{-1}$ and 79 $mAhg^{-1}$ and 102 $mAhg^{-1}$, respectively. This phenomenon might be due to the development of porosity in the activated carbon that could act as reservoirs for lithium storage, thus enhancing the electrochemical performance. Moreover, the first charge and discharge values of graphitic carbon (G–G′) were 132 $mAhg^{-1}$ and 115 $mAhg^{-1}$, respectively. Furthermore, the first charge and discharge profile for graphene material deliver the capacity of lithium insertion of 148 $mAhg^{-1}$ and a reversible charging capacity of 147 $mAhg^{-1}$. This might be due to the graphene-based structure possessing larger and more wrinkles of surface area as compared with graphite layers. The high surface area of the graphene-based materials can be considered responsible for the increased capability toward the electrolyte. In the other side, graphene-based material which is developed by Hummer's method could also generate more active sites throughout the surface for tethering the lithium ion. Wrinkled graphene layers consist of porous structures that could provide more lithium intercalation active sites. Previous research suggests the possibility of a reversible reaction between lithium and the residual hydrogen on the surface of graphene sheets and faradaic contribution also developed the enhancement of its capacity.[14] Several irreversible capacity phenomena that were observed in the first galvanostatic charge/discharge profiles of carbon-based

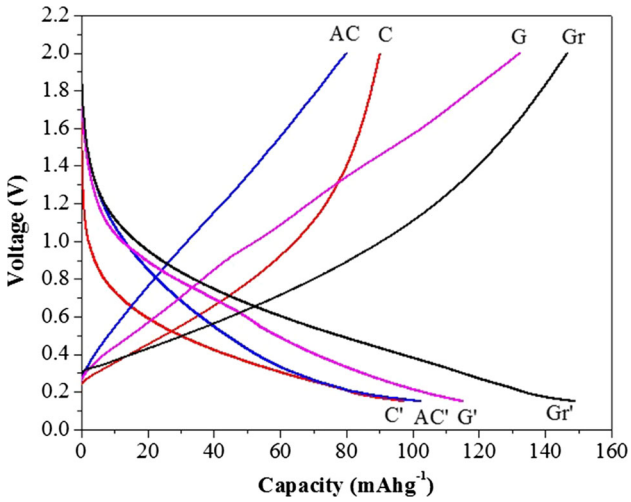

Fig. 5. The charge/discharge profile of the non-activated carbon (C–C′), activated carbon (AC–AC′), graphitic carbon (G–G′), and graphene (Gr–Gr′).

structures might be due to the development of SEI and some ionic reaction between lithium and developed-ionic substances throughout the surface of carbon-based materials. Moreover, these results indicate that the graphene-based material has good electrochemical performance. This result is in accordance with the previous investigation.[23]

Electrochemical characteristics, ionic transfer, electronical conductivity, and the resistance characteristics behavior were investigated through EIS measurement. Figure 6a and b shows the Nyquist plots with the potential ranging from 20 kHz to 0.1 Hz. It could be observed that the Nyquist plots exhibit one depressed semicircle and an inclined line at high to middle and low frequency, respectively. The inclined line with an angle around 45° to the axis indicated the process of lithium-ion diffusion in the carbon electrode. The value of the real axis intercept in the high-frequency range represents the equivalent series resistance (ESR), which is the resultant of the electrolyte resistance, the intrinsic resistance of the active electrode material, and the contact resistance at the interface between the current collector and the active materials.[30] A small semicircle indicates good capacitive performance and lower interfacial charge-transfer resistance on the electrode surface.[4,38] The ESR value of non-activated carbon, activated carbon, graphitic, and graphene-based material were 111 Ω, 76.8 Ω, 67.5 Ω, and 25.9 Ω, respectively. According to the ESR value, the graphene-based material exhibited the lowest ESR value. This might be related to the development of the two-dimensional flat layer of graphene that promote the simple and easy path for the faster delivery of ionic movement, thus increasing ionic conductivity. Additionally, from the Warburg impedance line, which was observed at low frequency, showed that graphene material exhibited the straighter line gradient, which indicated the faster diffusion process of lithium ions that hus enhanced the intercalation process of lithium ions into the graphene surface. This result indicated that the soybean waste-based carbon materials, especially after its transformation into graphene-based material, exhibited high electrochemical activity with low resistance and a good conductivity. Moreover, the electrochemical characterizations demonstrated that graphene-based material made by chemically treated graphite exhibited unique and excellent electrochemical properties in comparison with non-activated carbon, activated carbon, and graphite. Eventually, the results demonstrate that the soybean waste-derived advanced carbon frameworks, specifically in the form of graphene-based material present suitable morphologies and structures, which allow the electrolyte to accelerate ion transport in the porous frameworks and meanwhile enable carbon interconnected networks to serve as the effective route for electron diffusion.

Cycling performance of carbon-based materials is shown in Figs. 7 and 8. A cycle performance test was conducted with the increasing current rate of 0.2C (C/5), 0.5C(C/2), 1C, 2C, 4C, 6C, 8C and decreasing current rate to 4C and 1C in order to investigate the reversibility after the applications of the high current rate with the cycle number up to 40 cycles. As shown in Figs. 7 and 8, capacity value was fairly stable at each rate from 0.2C to 8C. Based on the cycle performance test, we could observe that graphene material was superior to others of carbon-based structure. The capacity value of graphene being much higher than the capacity of graphitic carbon, activated carbon and non-activated carbon. Figure 9 shows the cycling performance of resultant material at 2C. The specific capacity of graphene materials being much higher than the specific capacity values of other carbon-based materials. For instance, the average coulombic efficiency of the graphene material was about 100% with the capacity around 70 $mAhg^{-1}$ after 100 cycles which suggests the excellent stability of graphene materials during the relatively higher cycles applications.

Moreover, these results suggest that graphene-based material was developed with high reversible capacity, good cycle performance and high charge/discharge capability in comparison with other carbon structures. These phenomena might be due to increased conductivity and the surface area of graphene layer along with the development of less agglomeration among the layers of graphene material.[16] Eventually, the availability of soybean waste residue from the local foods market, especially in Indonesia, could reduce the total cost needed for the development of lithium-ion battery significantly, thus accelerate the technology expansion of lithium-ion batteries. In comparison with other biomass, soybean waste residue is easier to obtain without any additional preparation process. Moreover, in respect to the electronic and electrochemical performance of these developed materials and in

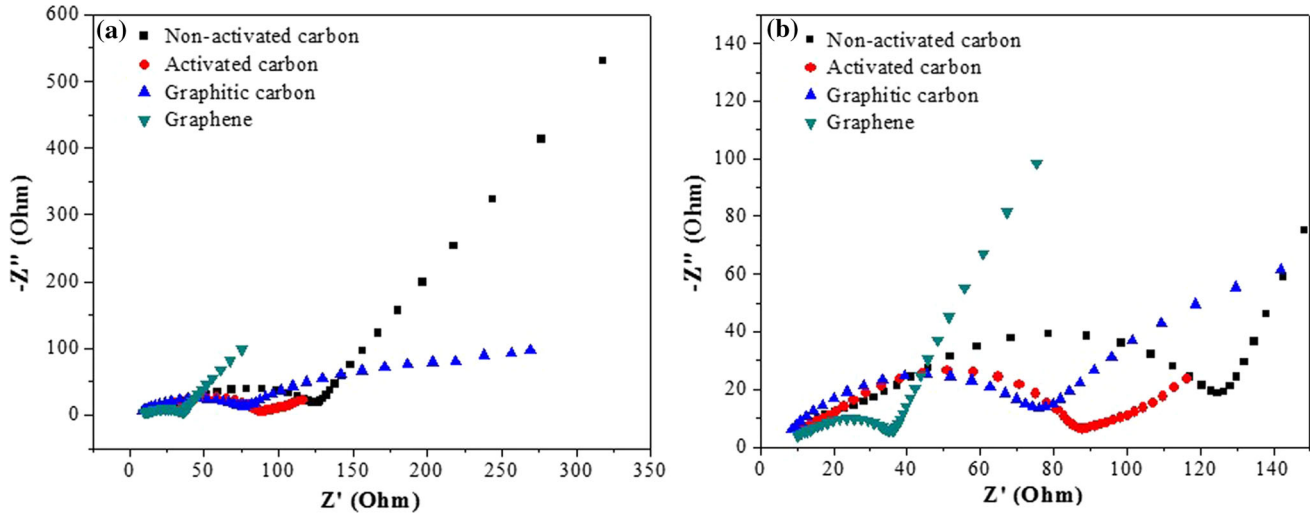

Fig. 6. Nyquist plots of (a) the non-activated carbon, activated carbon, graphitic carbon, graphene, and (b) their magnified images.

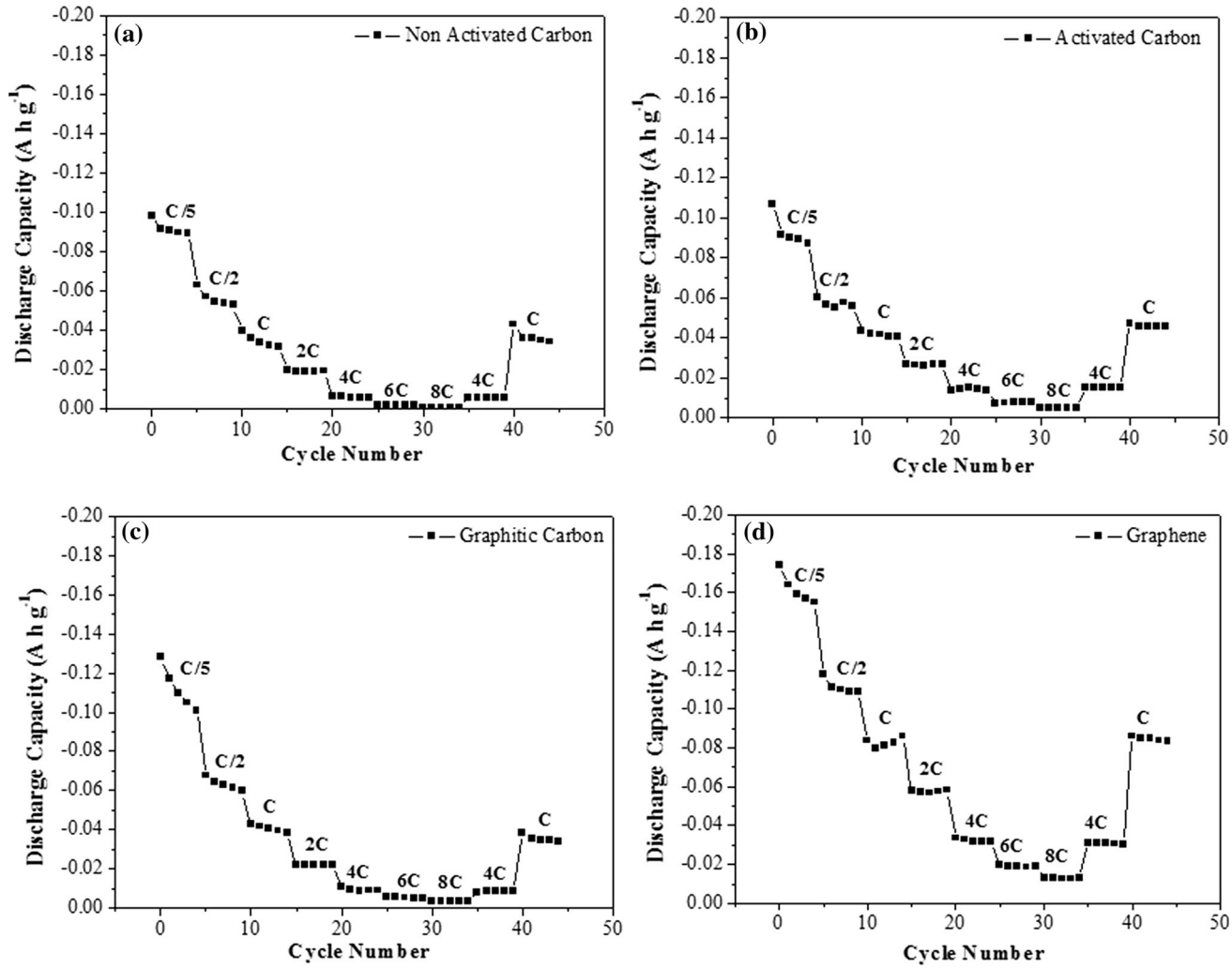

Fig. 7. Discharge capacity and cycle performance as a function of current rate of (a) nonactivated carbon, (b) activated carbon, (c) graphitic carbon, and (d) graphene.

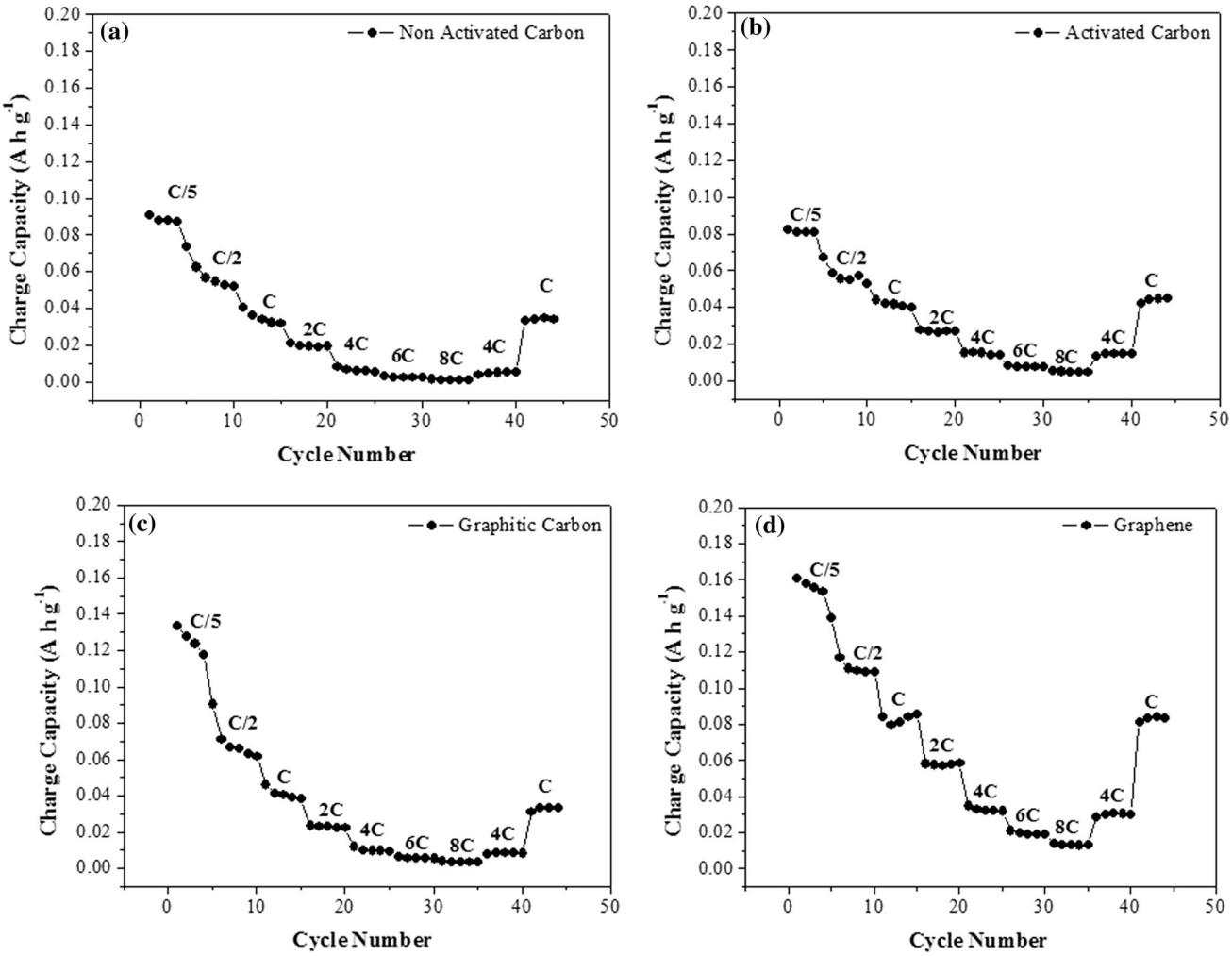

Fig. 8. Charge capacity and cycle performance as a function of current rate of (a) nonactivated carbon, (b) activated carbon, (c) graphitic carbon, and (d) graphene.

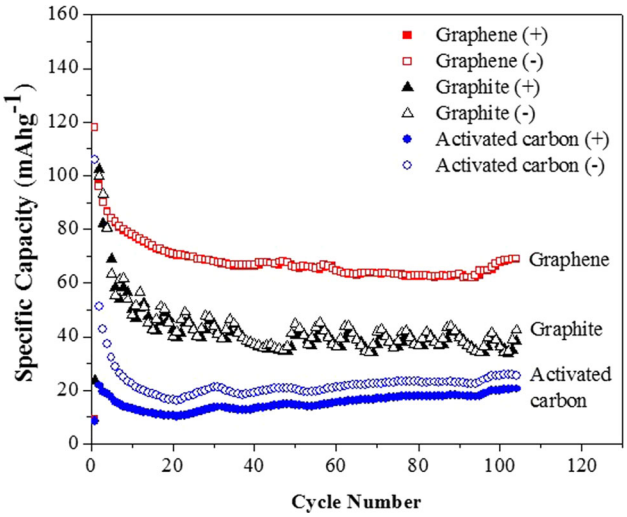

Fig. 9. Specific capacity of selected carbon-based materials; discharging (–) and charging (+).

order to enhance the capacity and performance of this novel material, several strategies for improvement and development are expected to be elaborated and investigated in the near future, for example, with some surface modification or synthesis process. The previous investigation reported the development of structures with graphene-based three-dimensional structures that could enhance the performance of graphene material for lithium-ion batteries applications.[16]

CONCLUSION

We have developed soybean waste as the main precursor for carbon-based advanced materials including non-activated carbon, activated carbon, graphitic carbon and graphene-based material through several processes including the heat treatment of the carbon precursor followed by a chemically-induced process. SEM results show that a

carbon-based material consists of layered and porous structures. Electrochemical impedance spectroscopy measurements show that graphene-based materials exhibit the lowest equivalent series resistance value of 25.9 Ω with high specific charge and discharge capacity of 147 $mAhg^{-1}$ and 148 $mAhg^{-1}$, respectively. Furthermore, in comparison with other developed structures, graphene material also exhibits high reversible capacity, good cycle performance, and a high rate charge/discharge capability. Eventually, these results confirmed that soybean waste could be developed as a potential precursor candidate for the development of competitive carbon-based advanced material, especially graphene-based material, for low-cost and high-performance energy storage devices, specifically for lithium-ion battery applications.

ACKNOWLEDGEMENTS

Financial support from the Indonesian Institute of Science Republic of Indonesia (No. 1139/F/2015) for this research is gratefully acknowledged.

CONFLICT OF INTEREST

The authors declare that they have no conflict of interest.

REFERENCES

1. Y. Shirazi, M.A. Tofighy, T. Mohammadi, and A. Pak, *Appl. Surf. Sci.* 257, 7359 (2011).
2. C.-G. Wang, X.-H. Shao, and R.-S. Xue, *J. Nanomater.* 2015, 5 (2015).
3. X. Yang, M. Li, N. Guo, M. Yan, R. Yang, and F. Wang, *RSC Adv.* 6, 4365 (2016).
4. J. Li, K. Liu, X. Gao, B. Yao, K. Huo, Y. Cheng, X. Cheng, D. Chen, B. Wang, W. Sun, D. Ding, M. Liu, and L. Huang, *ACS Appl. Mater. Interface* 7, 24622 (2015).
5. D. Avila-Brande, D. Arenas-Esteban, L.C. Otero-Diaz, A. Guerrero-Martinez, G. Tardajos, and J. Carretero-Gonzalez, *RSC Adv.* 5, 86282 (2015).
6. D. Jariwala, V.K. Sangwan, L.J. Lauhon, T.J. Marks, and M.C. Hersam, *Chem. Soc. Rev.* 42, 2824 (2013).
7. F. Karchemski, D. Zucker, Y. Barenholz, and O. Regev, *J. Control. Release* 160, 339 (2012).
8. M. Sevilla, C. Sanchís, T. Valdés-Solís, E. Morallón, and A.B. Fuertes, *Carbon* 46, 931 (2008).
9. X. Peng, J. Fu, C. Zhang, J. Tao, L. Sun, and P.K. Chu, *Nanosci. Nanotechnol. Lett.* 6, 68 (2014).
10. L. Sun, C. Tian, M. Li, X. Meng, L. Wang, R. Wang, J. Yin, and H. Fu, *J. Mater. Chem. A* 1, 6462 (2013).
11. Y. Zhu, S. Murali, M.D. Stoller, K.J. Ganesh, W. Cai, P.J. Ferreira, A. Pirkle, R.M. Wallace, K.A. Cychosz, M. Thommes, D. Su, E.A. Stach, and R.S. Ruoff, *Science* 332, 1537 (2011).
12. L.-Z. Fan, T.-T. Chen, W.-L. Song, X. Li, and S. Zhang, *Sci. Rep.* 5, 15388 (2015).
13. Q. Shao, J. Tang, Y. Lin, F. Zhang, J. Yuan, H. Zhang, N. Shinya, and L.-C. Qin, *J. Mater. Chem. A* 1, 15423 (2013).
14. P. Lian, X. Zhu, S. Liang, Z. Li, W. Yang, and H. Wang, *Electrochim. Acta* 55, 3909 (2010).
15. R.C. de Guzman, J. Yang, M.M.-C. Cheng, S.O. Salley, and K.Y. Simon Ng, *J. Mater. Sci.* 48, 4823 (2013).
16. Z. Hou, Z. Chen, M. Jing, H. Yang, G. Li, and M. Zhou, *J. Electron. Mater.* 47, 422 (2017).
17. C. Wang, D. Li, C.O. Too, and G.G. Wallace, *Chem. Mater.* 21, 2604 (2009).
18. R. Raccichini, A. Varzi, S. Passerini, and B. Scrosati, *Nat. Mater.* 14, 271 (2015).
19. P. Guo, H. Song, and X. Chen, *Electrochem. Commun.* 11, 1320 (2009).
20. E. Yoo, J. Kim, E. Hosono, H.-S. Zhou, T. Kudo, and I. Honma, *Nano Lett.* 8, 2277 (2008).
21. G. Wang, X. Shen, J. Yao, and J. Park, *Carbon* 47, 2049 (2009).
22. L. Tian, Q. Zhuang, J. Li, Y. Shi, J. Chen, F. Lu, and S. Sun, *Chin. Sci. Bull.* 56, 3204 (2011).
23. F. Zou, X. Hu, L. Qie, Y. Jiang, X. Xiong, Y. Qiao, and Y. Huang, *Nanoscale* 6, 924 (2014).
24. B. Xu, H. Wu, C.X. Lin, B. Wang, Z. Zhang, and X.S. Zhao, *RSC Adv.* 5, 30624 (2015).
25. W. Qian, F. Sun, Y. Xu, L. Qiu, C. Liu, S. Wang, and F. Yan, *Energy Environ. Sci.* 7, 379 (2014).
26. Z. Zhao, Y. Wang, M. Li, and R. Yang, *RSC Adv.* 5, 34803 (2015).
27. J. Li, G. Zan, and Q. Wu, *New J. Chem.* 39, 8165 (2015).
28. S.-J. Yuan and X.-H. Dai, *RSC Adv.* 5, 45827 (2015).
29. G.A. Ferrero, A.B. Fuertes, and M. Sevilla, *Sci. Rep.* 5, 16618 (2015).
30. Y.C. Chang and H.J. Sohn, *J. Electrochem. Soc.* 147, 50 (2000).
31. G. Ma, F. Ran, H. Peng, K. Sun, Z. Zhang, Q. Yang, and Z. Lei, *RSC Adv.* 5, 83129 (2015).
32. O. Akhavan, K. Bijanzad, and A. Mirsepah, *RSC Adv.* 4, 20441 (2014).
33. A.H. Mevold, W.W. Hsu, A. Hardiansyah, L.Y. Huang, M.C. Yang, T.Y. Liu, T.Y. Chan, K.S. Wang, Y.A. Su, R.J. Jeng, J.K. Wang, and Y.L. Wang, *Nanoscale Res. Lett.* 10, 397 (2015).
34. G. Ren, S. Li, Z.-X. Fan, J. Warzywoda, and Z. Fan, *J. Mater. Chem. A* 4, 16507 (2016).
35. S. Goswami, P. Banerjee, S. Datta, A. Mukhopadhayay, and P. Das, *Process Saf. Environ. Prot.* 106, 163 (2017).
36. S.S. Shams, L.S. Zhang, R. Hu, R. Zhang, and J. Zhu, *Mater. Lett.* 161, 476 (2015).
37. H. Liu, J. Huang, X. Li, J. Liu, and Y. Zhang, *J. Wuhan Univ. Technol. Mater. Sci. Ed.* 28, 220 (2013).
38. Y. Huang, S.L. Candelaria, Y. Li, Z. Li, J. Tian, L. Zhang, and G. Cao, *J. Power Sources* 252, 90 (2014).